



# Neutral silicon interstitials in silicon carbide: a first principles study

Ting Liao, Guido Roma, Jingyang Wang

► **To cite this version:**

Ting Liao, Guido Roma, Jingyang Wang. Neutral silicon interstitials in silicon carbide: a first principles study. *Philosophical Magazine*, Taylor & Francis, 2009, 89 (26), pp.2271-2284. <10.1080/14786430903055184>. <hal-00514031>

**HAL Id: hal-00514031**

**<https://hal.archives-ouvertes.fr/hal-00514031>**

Submitted on 1 Sep 2010

**HAL** is a multi-disciplinary open access archive for the deposit and dissemination of scientific research documents, whether they are published or not. The documents may come from teaching and research institutions in France or abroad, or from public or private research centers.

L'archive ouverte pluridisciplinaire **HAL**, est destinée au dépôt et à la diffusion de documents scientifiques de niveau recherche, publiés ou non, émanant des établissements d'enseignement et de recherche français ou étrangers, des laboratoires publics ou privés.



**Neutral silicon interstitials in silicon carbide: a first principles study**

Journal:	<i>Philosophical Magazine &amp; Philosophical Magazine Letters</i>
Manuscript ID:	TPHM-08-Nov-0433.R1
Journal Selection:	Philosophical Magazine
Date Submitted by the Author:	20-Jan-2009
Complete List of Authors:	Liao, Ting; IMR, High Performance Ceramic Division; CEA-Saclay, Service de Recherches de M�tallurgie Physique Roma, Guido; CEA-Saclay, Service de Recherches de M�tallurgie Physique Wang, jingyang; IMR, High Performance Ceramic Division
Keywords:	defects, diffusion, first-principles calculations, silicon carbide
Keywords (user supplied):	defects, diffusion, first-principles calculations



# Neutral silicon interstitials in 3C- and 4H-SiC:

## A first-principles study

Ting Liao<sup>1,2,3</sup>, Guido Roma<sup>1,\*</sup> and Jingyang Wang<sup>2</sup>

1 Service de Recherches de Métallurgie Physique, CEA Saclay, 91191 Gif sur Yvette, France

2 High-performance Ceramic Division, Shenyang National Laboratory for Materials Science, Institute of Metal Research, Chinese Academy of Sciences, Shenyang, 110016, China

3 Graduate School of Chinese Academy of Sciences, Beijing, 100039, China

**Abstract.** The structures and stability of single silicon interstitials in their neutral state are investigated via first principles calculations in 3C- and 4H-SiC. By carefully checking the convergence with Brillouin Zone (BZ) sampling and supercell size we explain the disagreement between previous published results and we show that the split interstitial along  $\langle 110 \rangle$  direction and tetrahedrally carbon coordinated structure have competing formation energies in the cubic polytype. A new migration mechanism for the silicon interstitial in the neutral state is presented here which could be important for the evolution of defect populations in SiC. For 4H-SiC, the most energetically favourable silicon interstitial is found to be the split interstitial configuration  $I_{\text{Sisp}\langle 110 \rangle}$  but situated in the hexagonal layer. The defect formation energies in 4H-SiC are in general larger than those in 3C-SiC, implying that the insertion of silicon interstitial introduces a large lattice distortion to the local coordination environments and affect even the second- or third-nearest neighbours. We also present a comparison between well converged plane waves calculations and calculations with three localized orbital basis sets; one of them, in spite of providing a reasonable description for bulk properties, is clearly not suitable to describe interstitial defects.

**Keywords:** Defects, Diffusion, First principles calculations, silicon carbide

### 1. Introduction

Silicon carbide (SiC) is a wide band-gap semiconductor ideally suited for high-temperature, high-power, and high-frequency applications [1], and its composites have been proposed for

---

\* Corresponding author

1  
2 structural components in future nuclear fusion reactors [2, 3], because of their high temperature  
3 strength, pseudo-ductile fracture behaviour, and low-induced radioactivity. In order to assess the  
4 performance of SiC-based components in radiation or ion implantation environments, a detailed  
5 understanding of the influence of defects on their structure and behaviour is necessary.  
6  
7

8  
9 Other domains of the application of silicon carbide include very high temperatures and  
10 irradiation environments where, in spite of their relatively high formation energies, silicon  
11 interstitials are expected to be present in high concentrations and will be important, maybe even  
12 crucial, in order to understand the behaviour of the material and its evolution. Indeed their  
13 mobility is expected to be high and they may play an important kinetic role [4] in the  
14 microstructural evolution. Furthermore, the amorphous SiC created by irradiation is known to  
15 include a large percentage of homopolar bonds, but its details are not yet fully understood [5-7].  
16  
17

18  
19 Theoretical studies of point defects in SiC have been widely performed using accurate density  
20 functional theory (DFT) [4,8-13], but relatively few studies regarding silicon interstitials have  
21 been published so far [4,10-12]; furthermore, some discrepancies between published results  
22 need a clarification. Indeed, depending on the variation of supercell size and  $k$ -point sampling,  
23 different formation energies have been reported so far for silicon interstitials in SiC. Defect  
24 energies calculated from DFT are expected to be quite accurate, nevertheless in several cases it  
25 has been shown that a higher level of theory than for the description of the bulk material is  
26 necessary [14-15]. We noticed that in the cited studies for silicon interstitials, in spite of  
27 different cell sizes used, the  $k$ -point samplings are almost all limited to the  $\Gamma$  point. Our  
28 results show that, even for supercells larger than all those used up to know,  $\Gamma$  point sampling  
29 is a source of large errors. In addition, our extensive comparison of plane waves based  
30 calculations with localised orbitals based ones shows that discrepancies can be non negligible  
31 on formation energies. Finally, we have found a mechanism for migration of the neutral silicon  
32 interstitial whose migration barrier is lower than previously reported.  
33  
34

35  
36 The paper is organized as follows: the computational details are described in section 2. In  
37 section 3 we present results for the formation energies of silicon interstitials in both 3C- and  
38 4H-SiC. The dependence of the defect formation energy on the  $k$ -point choice and supercell  
39  
40  
41  
42  
43  
44  
45  
46  
47  
48  
49  
50  
51  
52

size, along with the description of local coordination environments of each interstitial type, is also illustrated in this section, as well as the migration mechanism in 3C-SiC. Finally, the concluding remarks are given in section 4.

## 2. Computational details

To determine the relative stability of different interstitial configurations, we compared their defect formation energies and, for this, we follow the standard formalism outlined in several previous studies to define reasonable bounds on the chemical potentials and to investigate the defect energies within these limits [16-18]. As a reminder, the formation energy of a neutral defect in SiC is hence defined as

$$E_f = E_{def} - n_{Si}\mu_{Si} - n_C\mu_C$$

(1)

Here, the chemical potentials  $\mu_i$  are not independent  $\mu_{SiC}$  but related to the chemical potential of bulk SiC, , i.e.,  $\mu_{Si} + \mu_C = \mu_{SiC}$ , and  $n_i$  is the number of atoms of type  $i$  added or removed to form the defect.

$E_{def}$  is the difference in energy between the supercell with and without the defect.

The analysis of the silicon interstitials was carried out by means of total energy calculations within the framework of Density Functional Theory (DFT), and by simulating the relevant interstitials using periodic supercells containing 64 and 72 atoms, respectively, for 3C- and 4H-SiC. We also enlarged the supercells of 3C-SiC to 128-, 216- and 512-atom to investigate the effects of the choices of supercell sizes as well as the  $k$ -point sampling on the results. The energies and forces calculations were performed using two codes with different basis sets, PWSCF (Plane Wave Self Consistent Field) using plane waves [19] and SIESTA (Spanish Initiative for Electronic Simulations with Thousands of Atoms) with linear combination of atomic orbitals [20]. In plane-wave PWSCF calculations we used ultrasoft and norm-conserving pseudopotentials to replace the core electrons of C and Si atoms, respectively. In most of the calculations, to provide sufficiently well-converged results, a  $2 \times 2 \times 2$  shifted Monkhorst-Pack

1  
2  
3  
4  
5  
6  
7  
8  
9  
10  
11  
12  
13  
14  
15  
16  
17  
18  
19  
20  
21  
22  
23  
24  
25  
26  
27  
28  
29  
30  
31  
32  
33  
34  
35  
36  
37  
38  
39  
40  
41  
42  
43  
44  
45  
46  
47  
48  
49  
50  
51  
52  
53  
54  
55  
56  
57  
58  
59  
60

$k$ -point mesh was used for the sampling of the Brillouin Zone. The exchange correlation energy is calculated in the Local Density Approximation (LDA). We employed a plane-wave cutoff energy of 30 Ry for energy calculations which is sufficient to achieve a full convergence of  $2 \times 10^{-2}$  eV/atom on total energies. We found no need to raise the charge density cutoff above 120 Ry. The atomic positions are relaxed until the Hellman-Feynman force on each atom is reduced to within  $10^{-3}$  Ry/Bohr ( $2.6 \times 10^{-2}$  eV/Å).

SIESTA calculations were also done within LDA for bulk and defected structures. The core electrons were replaced by [norm-conserving](#) pseudopotentials [generated by Troullier and Martins](#)[21]; valence electrons were described by three basis sets: a double- $\zeta$  polarized (DZP) basis set, a triple- $\zeta$  one without polarization (TZ), and a triple- $\zeta$  basis set including polarization for silicon orbitals (TZP) [22].

More details for the comparison of the basis sets, including equilibrium bulk properties, are in table 1. A  $2 \times 2 \times 2$  shifted  $k$ -points mesh and 80 Ry grid cutoff were adopted for all energy calculations, unless stated otherwise. The convergence tolerance for the geometry optimization was a maximum Hellmann-Feynman force within 0.01 eV/Å.

Deleted: Troullier-Martins

Deleted: according to the recipe

### 3. Results and discussion

#### 3.1. Formation energy and convergence issues for silicon interstitials in 3C-SiC

The crystallographic structure 3C-SiC is of the zinc-blend type; it consists of zigzag chains when regarded along the  $\langle 110 \rangle$  direction and it can be described as a stacking of atomic planes with hexagonal symmetry in the sequence of ABCABC along the  $\langle 111 \rangle$  axis of the conventional cubic cell. For the modelling of the interstitial defects in this type of structure, we place the interstitial atoms in the regions with open space and in the form of split-interstitial configurations distinguished by the crystallographic symmetry and the local environments (see red balls in figure 1), and perform relaxation to allow for the minimization of the forces and stresses. As depicted in figure 1, different starting interstitial configurations have been explored for 3C-SiC: the tetrahedrally coordinated interstitial sites, with either a four silicon ( $I_{TSi}$ ) or four

1  
2 carbon ( $I_{TC}$ ) nearest neighbors; a hexagonal configuration  $I_{Hex}$ , where the interstitial atom is  
3 located in the center of a hexagon of alternating silicon and carbon atoms; various split  
4 interstitial configurations sharing either carbon or silicon lattice site, occurring with orientations  
5 in the  $\langle 100 \rangle$ , the  $\langle 110 \rangle$  and the  $\langle 111 \rangle$  directions; furthermore we considered a bond-center  
6 configuration where the interstitial silicon is centered at the heteropolar bond of two nearest  
7 neighbouring lattice atoms.  
8

9  
10 The calculated results of the silicon interstitial formation energies of 3C-SiC in the two extreme  
11 chemical potential conditions are tabulated in table 2. The results in here are obtained by  
12 variable-cell optimization, which partially relieves the elastic energy arising from the  
13 crystallographic distortion induced by the defect. The ordering according to formation energy of  
14 the various configurations is the same for the PWSCF plane waves calculations and the SIESTA  
15 with basis sets DZP and TZP. The TZ unpolarized basis set gives much higher formation  
16 energies. In the following we will mainly comment on SIESTA calculation with the DZP basis,  
17 as they are more efficient than the TZP and give results which are almost as close to the PW  
18 results as the TZP ones. As can be seen from table 2, silicon interstitials in 3C-SiC respond  
19 strongly to the different local coordination environments and the hierarchy of silicon interstitials  
20 also depends on it. Here, the most stable configuration is the dumbbell-like split interstitial on a  
21 silicon site along  $\langle 110 \rangle$  direction ( $E_f = 8.40$  eV) followed by the tetrahedrally  
22 carbon-coordinated interstitial  $I_{TC}$  ( $E_f = 8.98$  eV). We refer to formation energies in silicon rich  
23 conditions, unless stated otherwise. This result is in disagreement with prior calculations also  
24 using plane-wave pseudopotential methods [10-11], which find  $I_{TC}$  to be the most favourable Si  
25 interstitial ( $E_f = 6.00$  eV) and obtain for the  $I_{Sisp\langle 110 \rangle}$  a formation energy which is 1.40 eV higher.  
26 We noticed that the two calculations, using 128 and 64 atom supercells respectively, both  
27 sampled the Brillouin-zone with the  $\Gamma$  point only. The work by Salvador *et al* [12], with a larger  
28 supercell containing 216 atoms, still with  $\Gamma$  point sampling, gives a formation energy of 6.7 eV  
29 for the carbon-coordinated interstitial  $I_{TC}$ , consistent with the result from Lento *et al.*, and  
30 suggesting a well converged result in these works, at least under the  $\Gamma$  point sampling condition.  
31 However, by employing a 64-atom cell and a denser  $k$ -point sampling ( $2 \times 2 \times 2$  shifted mesh), an  
32  
33  
34  
35  
36  
37  
38  
39  
40  
41  
42  
43  
44  
45  
46  
47  
48  
49  
50  
51  
52  
53  
54  
55  
56  
57  
58  
59  
60

1  
2 agreement can be found on the formation energies of  $I_{\text{Sisp}\langle 110 \rangle}$  in the neutral state between our  
3 results and those from M. Bockstedte *et al* [4]. All the cited works are results of plane waves  
4 pseudopotential calculations.  
5

6  
7 More recently it has been shown that in semiconductors, like silicon and diamond, even if  
8 energy differences are calculated between values obtained with equivalent supercell sizes and  
9  $k$ -point sampling, the error in formation energies caused by the limitation of  $k$ -point sampling  
10 will not be easily cancelled out [23]. It is thus necessary to check the effect of the choice of  
11  $k$ -point sampling on the energy convergence of defect-containing structures. It is worth restating  
12 that we are using supercells in order to simulate an isolated defect. The fact that  $k$ -point  
13 sampling of the BZ has to be carefully considered comes from two reasons: first, the screening  
14 in the bulk material has to be correctly described; second, the defect levels themselves can show  
15 a dispersion with  $k$ . The latter means that our defect periodic images are interacting and there is  
16 an error coming from the finite size of the supercell, in spite of the convergence with  $k$ -point  
17 sampling.  
18

19  
20 In figure 2a, we compare the convergence of defect formation energies of  $I_{\text{TC}}$  and  $I_{\text{Sisp}\langle 110 \rangle}$  in  
21 3C-SiC structures in terms of different  $k$ -point samplings for the 65- and 129-atom supercells  
22 with fully relaxed atomic positions at constant volume. Here, we obtained a formation energy  
23 for  $I_{\text{TC}}$  in close agreement with the value from Lento *et al.* based on the same calculation  
24 conditions (at  $\Gamma$  point and for 128-atom supercell). As shown in figure 2a, the convergence  
25 with increasing  $k$ -point density is slow and, in particular, the formation energy for  $I_{\text{Sisp}\langle 110 \rangle}$   
26 defect converge more quickly than the interstitial  $I_{\text{TC}}$  does; in other words, the latter defect  
27 responds more sensitively to the choice of  $k$  points. With increasing  $k$  grid density, the formation  
28 energies of  $I_{\text{TC}}$  and  $I_{\text{Sisp}\langle 110 \rangle}$  finally converged at 8.92 and 8.67 eV, in a 128 atoms supercell.  
29

30  
31 We also remark that, as suggested previously [24], the only fact of using another  $k$ -point  
32 —( $1/2, 1/2, 1/2$ ) for cubic cells and ( $1/4, 1/4, 1/4$ ) for FCC cells— instead of  $\Gamma$  allows to obtain almost  
33 converged values.  
34

35  
36 We now discuss the other main source of error, which is the limited size of the supercell. We  
37 performed the atomic relaxation of the  $I_{\text{TC}}$  and  $I_{\text{Sisp}\langle 110 \rangle}$  structures considering both  $\Gamma$  only and  
38



1  
2 converged  $k$ -point samplings, respectively, by increasing the cell size up to 512-atom. The  
3 results are shown in figure 2b. As the size of the supercell increases the formation energies for  
4 both defect configurations calculated using the  $\Gamma$ -point sampling increase significantly. When  
5 converged with respect to the  $k$ -point sampling the formation energy for the split configuration  
6 seems well converged already with a 65 atoms supercell, but for the tetrahedral one the energy  
7 still decreases, reminding of the case of the vacancy in silicon [23].

8  
9 This behaviour can be rationalized by a closer look into the electronic structure of these defects.  
10 Indeed the  $T_C$  position, in the 65 atoms supercell, has occupied levels above the conduction  
11 band edge, which means that the system becomes metallic (or that this defect is expected to be  
12 positively charged at any doping condition). This effect could be an artifact of the well known  
13 underestimation of the band gap by DFT-LDA calculations. In some cases in which the DFT  
14 band structures are even qualitatively different from experimental excitations spectra, total  
15 energies and structural properties are relatively well described. Let us mention the example of a  
16 Mott insulator: uranium dioxide [25]. [However our findings warn about the possible errors of](#)  
17 [standard DFT approaches even for neutral defects in solids whose ground state properties are](#)  
18 [believed to be relatively well described.](#) In conclusion, the interstitials configurations  $I_{TC}$  and  
19  $I_{Sisp<110>}$  are very close in formation energy and separated by at most a few tenth of an eV, in  
20 [DFT-LDA](#). Our best converged results (8.12 and 8.27 eV respectively) were obtained with a  
21 512-atom supercell and  $2 \times 2 \times 2$  shifted  $k$ -point mesh.

22  
23  
24  
25  
26  
27  
28  
29  
30  
31  
32  
33  
34  
35  
36  
37  
38  
39  
40  
41  
42  
43  
44  
45  
46  
47  
48  
49  
50  
51  
52  
53  
54  
55  
56  
57  
58  
59  
60

The split interstitials at silicon site with  $\langle 100 \rangle$  and  $\langle 111 \rangle$  orientations have higher formation energies than  $I_{TC}$  and  $I_{Sisp<110>}$ , and the tetrahedrally silicon-coordinated interstitial  $I_{TSi}$  turns out to be the least stable one in all investigated interstitial configurations. These three configurations, which have metallic character as  $I_{TC}$ , are either very shallow minima or even saddle points, because a very small perturbation, releasing the symmetry constraints, allows the configuration to switch to the  $I_{Sisp<110>}$  configuration with practically no barrier. These three almost unstable configurations can then provide migration mechanisms with migration energies (1.5-2.5 eV) similar or higher than those reported by Bockstedte [4] for neutral species.

The effect of the insertion of silicon interstitials on the relative volume changes after relaxation

Deleted: However, i

Deleted: everal

Deleted: .

1  
2 is also presented in table 2. The interstitials in the split-interstitial form produce a comparatively  
3 larger expansion of the crystalline volume and such distortion make the defects less symmetric,  
4 whereas others, such as the carbon- and silicon-coordinated interstitial configuration, have a  
5 much smaller effect and their volume expansion after a full relaxation was 0.99 % and 1.29 %,  
6 respectively. This suggests that the slow convergence with cell size for  $I_{TC}$  is not related to the  
7 elastic interactions between defect periodic images. SIESTA calculations yields in general  
8 slightly larger volumes expansion, and even much larger for the TZ basis sets (up to more than  
9 four atomic volumes).

### 19 3.2. Local environments of silicon interstitials in 3C-SiC

20 In table 2, interstitial atoms and the nearby atoms are shown at relaxed positions for 3C-SiC,  
21 including a summary of relaxed local bond lengths for the interstitials. The criterion for bonding  
22 is chosen to be the atomic distances with the upper thresholds of 2.40 Å for Si-Si bonds and  
23 1.90 Å for Si-C bonds. Although supercells of each type dilate accordingly with the silicon  
24 insertion, the changes in bond lengths for each defect have to be understood in terms of local  
25 coordination environments and charge effects. For the tetrahedrally coordinated interstitials  
26 surrounded by carbon or silicon atoms,  $T_d$  symmetry is kept, with some differences from the  
27 relaxation pattern of the nearest atoms. For  $I_{TSi}$ , the nearest silicon atoms move slightly away  
28 from the interstitial site, whereas in  $I_{TC}$  the four carbon first neighbours move slightly closer.  
29 The tetrahedron formed by these carbon atoms undergoes a volume contraction of around 7%,  
30 while the octahedron formed by the six silicon second-neighbours get strongly dilated (~30% in  
31 volume). The latter constitutes the main contribution to the volume expansion induced by the  $T_C$   
32 interstitial.  
33

34 Due to the open structure of the SiC along the  $\langle 110 \rangle$  direction, the split interstitial configuration  
35 with this orientation can easily release the strain energy. The starting configurations with split  
36 interstitials at carbon site along  $\langle 110 \rangle$  and  $\langle 111 \rangle$  directions and with the silicon atom residing  
37 in the center of a hexagon of alternating silicon and carbon atoms are unstable, and they all relax  
38  
39  
40  
41  
42  
43  
44

down to the tetrahedrally carbon-coordinated symmetry ultimately. Besides all these well documented silicon interstitial configurations, another different point defect pattern in the form of a combination of antisite  $\text{Si}_\text{C}$  plus a carbon split interstitial  $\text{I}_{\text{CspSi}}$  on a silicon site was also found in our study. This result was obtained with a slight torsion of the Si-C bonds surrounding the hexagonal interstitial site, and a three-membered ring was formed encircled by the antisite defect and the split pair. This defect complex is also a relatively low-energy defect structure of silicon interstitial with a formation energy equal to 9.27 eV (Si-rich conditions). Compared to the others silicon interstitial structures, this defect complex is only less stable than the  $\text{I}_{\text{TC}}$  and  $\text{I}_{\text{Sisp}\langle 110 \rangle}$ , and could play a role in the energy landscape of silicon interstitials.

### 3.3. A mechanism for the migration of silicon interstitials in 3C-SiC

Interstitial mobility is known to be higher than that of vacancies in SiC [4]. In the presence of Si self-interstitials, the identified almost equally stable configurations,  $\text{I}_{\text{TC}}$  and  $\text{I}_{\text{Sisp}\langle 110 \rangle}$ , might transform into one another by thermal activation. We estimated the barrier of this transition by searching the minimum energy path between  $\text{I}_{\text{TC}}$  and  $\text{I}_{\text{Sisp}\langle 110 \rangle}$  in their neutral state. The path, generated using the nudged elastic band (NEB) [26] method as implemented in PWSCF, is depicted in figure 3 for the 4x4x4 FCC supercell (containing 128 atoms). The process which transforms  $\text{I}_{\text{TC}}$  into  $\text{I}_{\text{Sisp}\langle 110 \rangle}$  and vice versa is not exceeding 0.85 eV. As an approximate evaluation of the error due to supercell size limitation for the migration barrier we have calculated the energy path with and without smearing of the Fermi surface; the difference of the two curves at the saddle point is of 0.1 eV. [The influence of the smearing of the Fermi surface, for which we adopted the cold-smearing scheme proposed by Marzari and coworkers \[27\], is negligible: for the  \$\text{I}\_{\text{TC}}\$  configuration, the calculated result with a smearing width of 0.005 Ry \(presented in figure 3\) differs by 0.02 eV with respect to the one with a smearing of 0.0001 Ry.](#)

We performed further calculations with a 217 atoms cubic supercell that confirm a migration energy between 0.7 and 0.8 eV. For this migration path, starting with  $\text{I}_{\text{TC}}$ , the silicon interstitial begins with a hop away from the tetrahedral interstice and pushes the nearby silicon atom out of its normal site to form a distorted intermediate split interstitial in a direction close to  $\langle 100 \rangle$ .

Formatted: Subscript

Deleted: ion

Deleted: r

Deleted: ,

1  
2 After this, a collective displacement of these two atoms toward the final  $I_{\text{Sisp}}\langle 110 \rangle$  dumb-bell  
3 takes place, until equilibrium is reached, while all other atoms relax only slightly during the  
4 diffusion event. To the best of our knowledge this migration mechanism of neutral silicon  
5 interstitials has definitely the lowest activation energy than all the previously reported ones [4];  
6 it should be the dominant mechanism for Si self-diffusion in compensated and *n*-type SiC,  
7 according to the charge transition levels calculated in [4].  
8  
9  
10  
11  
12

### 13 14 15 16 3.3. Relative stability of silicon interstitials in 4H-SiC

17 The crystal structure of 4H-SiC can be described as the alternating cubic and hexagonal stacking  
18 sequence arranged along *c*-axis in a form of ABCBABC. The higher number of non-equivalent  
19 lattice sites in 4H-SiC leads to a greater variety of potential elementary interstitial defect than in  
20 3C-SiC. Having recognized the instability of silicon split-interstitial on carbon site for 3C-SiC,  
21 we did not consider this insertion site in 4H-SiC. The investigated initial silicon interstitial  
22 configurations in 4H-SiC are all displayed in figure 4. As in 3C-SiC the cubic lattice layer  
23 enclose both the tetrahedrally carbon and silicon coordinated sites. In the hexagonal layer,  
24 interstitial site  $I_{\text{TCSi}}$  is characterized by a tetrahedral surrounding by four carbon and four silicon  
25 atoms, and  $I_{\text{Hex(CSi)}}$  is in an open cage encompassed by two hexagonal rings of the lower and  
26 upper basal plane. Another hexagonal configuration  $I_{\text{Hex}}$ , which resembles that in 3C-SiC is  
27 located in the center of a hexagon of alternating silicon and carbon atoms. For the split  
28 interstitials in 4H-SiC, they can be located entirely within a basal plane considering different  
29 orientations of  $\langle 10\bar{1}0 \rangle$  or  $\langle 1\bar{2}10 \rangle$ .  
30  
31  
32  
33  
34  
35  
36  
37  
38  
39  
40  
41

42 In addition, other split interstitial configurations resembling the crystallographic geometry in  
43 3C-SiC along  $\langle 100 \rangle$  or  $\langle 110 \rangle$  directions are also taken into account. All the split interstitial  
44 patterns apply to the lattice sites in the cubic layer as well as in the hexagonal layer.  
45  
46

47 Table 3 summarizes the calculated formation energy of all investigated stable interstitials in  
48 4H-SiC for C- and Si-rich limits. They were obtained with a 3x3x1 supercell containing 72(+1)  
49 atoms and 3x3x1 *k*-point mesh. The most energetically favourable interstitial configuration in  
50  
51  
52  
53  
54  
55  
56  
57  
58  
59  
60

1  
2 4H-SiC is the split interstitial with  $\langle 110 \rangle$  orientation on the silicon atom site, which locates in  
3 the hexagonal layer.  
4

5 A similar Si-Si split with the same orientation in the cubic region turns out to be less stable by  
6 0.87 eV. In particular, this split pair in the cubic layer provokes stronger distortion of the  
7 simulation supercell and induces a larger volume expansion by 0.3 % than the pair does in the  
8 hexagonal region. On the basal plane, split interstitials along  $\langle 10\bar{1}0 \rangle$  and  $\langle 1\bar{2}10 \rangle$   
9 crystallographic orientations result in different interstitial configurations. Both dumbbell  
10 configurations with  $\langle 10\bar{1}0 \rangle$  symmetry in cubic and hexagonal planes exhibit almost identical  
11 stability due to the similar nearest-neighbour environments which allow for similar relaxation  
12 pattern. Their defect formation energies differ from one another negligibly, although a switch of  
13 comparative orders is observed changing from the TZP basis set (in agreement with plane  
14 waves) to the DZP or TZ basis sets. In the cases of  $\langle 1\bar{2}10 \rangle$ -oriented configurations, even  
15 without a perturbation, these two split interstitials turn out to be very unstable and re-orientate  
16 their directions into  $\langle 100 \rangle$  and  $\langle 110 \rangle$ , respectively, in cubic and hexagonal layers. Let us  
17 emphasize that the  $\langle 100 \rangle$  orientation, which turned out to be metallic in the cubic polytype, has  
18 its highest occupied band inside the gap, thanks to the larger band gap of 4H-SiC. We expect  
19 then, in general, the size effect to be much smaller for the 4H polytype than for the 3C.  $I_{TCub}$ ,  
20 which is characterized by a tetrahedral site surrounded by four carbon atoms in the cubic layer,  
21 is the least favourable stable configuration in 4H-SiC and is unstable if relaxed with SIESTA  
22 and the TZ basis set. The two other tetrahedral configurations,  $I_{TCSi}$  and  $I_{TSicub}$ , turn out to be  
23 unstable.  
24  
25  
26  
27  
28  
29  
30  
31  
32  
33  
34  
35  
36  
37  
38  
39  
40

41 When comparing the relaxed structures of the interstitial atoms and their nearby atoms in  
42 4H-SiC, as shown in table 3, we notice that, despite the complexity of non-equivalent lattice  
43 site, many relaxed interstitial structures share the same spatial symmetry characteristics, for  
44 example, the obtained stable split-interstitial configurations all have a symmetry of  $C_s$ , and the  
45 others are classified into the pattern  $C_{3v}$  holding the most typical three-axis rotation symmetry in  
46 hexagonal 4H-SiC. It is also interesting to notice that the relaxed positions of silicon interstitial  
47  
48  
49  
50  
51  
52

1  
2 in the hexagonal region encompassed by two hexagonal rings, which are named as  $I_{\text{Hex}}$  and  
3  
4  $I_{\text{Hex(CSi)}}$ , are so close to one another that, with a tiny perturbation the less stable configuration  
5  
6  $I_{\text{Hex}}$  will change to  $I_{\text{Hex(CSi)}}$  with great ease by sliding down the potential energy surface.  
7  
8

#### 9 10 **4. Conclusions**

11 The energies of silicon interstitials in 3C- and 4H-SiC have been calculated from first principles  
12 by exploring a variety of possible configurations. The stable interstitial configurations have  
13 been characterized by formation energies and formation volumes.  
14  
15

16 We clarified that discrepancies between previously published results are due to limitations in  
17 supercell size and/or  $k$ -point sampling. In particular, the determination of the most stable  
18 position of the neutral silicon interstitial in cubic SiC is very delicate, showing a competition  
19 between the split interstitial sharing a silicon lattice site along  $\langle 110 \rangle$  orientation and the  
20 tetrahedral position surrounded by carbon atoms. In the hexagonal polytype the former is clearly  
21 the most stable position. The formation energies for the most stable configurations are all above  
22 8 eV.  
23  
24  
25  
26  
27  
28  
29

30 The comparison between the two polytypes (3C and 4H) shows similar formation energies, in  
31 general higher for the hexagonal polytype, if we compare similar configurations. We also  
32 compare well converged results obtained with a plane waves basis sets with the outcome of  
33 SIESTA calculations using different localized basis set. The best compromise seems to be a  
34 double- $\zeta$  polarized basis set. The stability order of the various configurations is almost always  
35 the same as with plane waves, the formation energies are similar, but the differences can be as  
36 large as 0.5 eV. The SIESTA calculations give lower formation energies than plane waves for  
37 the 4H polytype but higher than plane waves for the cubic one. Nevertheless the trend showing  
38 higher formation energies in the hexagonal polytype is maintained.  
39  
40  
41  
42  
43  
44  
45

46 We have found a diffusion mechanism for the silicon interstitial in cubic SiC, consisting in hops  
47 between split and tetrahedral configurations; the corresponding migration energy is estimated at  
48 0.8 eV, lower than previously reported ones [4]. This point suggests that silicon interstitials  
49  
50  
51  
52  
53  
54  
55  
56  
57  
58  
59  
60

1  
2 could play a role more important than expected in the evolution of defects populations in SiC  
3  
4 under irradiation.  
5  
6

### 7 8 **Acknowledgements**

9  
10 We are grateful to Yanchun Zhou and the Institute of Metal Research (Shenyang, China) for  
11 making possible the one year stay of T.L. at CEA-Saclay during her PhD period in the  
12 framework of the collaboration between our two laboratories. We also wish to acknowledge the  
13 support of CCRT (Centre de Calcul de Recherche et Technologie) for the computing time  
14 allocated through the partnership with CEA Nuclear Energy Division (DEN).  
15  
16  
17  
18  
19  
20

### 21 **References**

- 22  
23 [1] S. Dimitrijevic and G. Jamet G, *Microelectron. Reliab.* 43 (2003) p.225-233  
24  
25 [2] G. R. Hopkins *Silicon Carbide and Graphite Materials for Fusion Reactors* Proc. IAEA  
26 Symp. Plasma Phys. and Controlled Nucl. Fusion Res., Tokyo, Japan, International Atomic  
27 Energy Agency IAEA-CN-33/s3-3, 1974.  
28  
29 [3] A. Hasegawa, A. Kohyama, R.H. Jones, L. L. Snead, B. Riccardi and P. Fenici, *J. Nucl.*  
30 *Mater.* 283 (2000) p.128-137  
31  
32 [4] M. Bockstedte, A. Mattausch and O. Pankratov, *Phys. Rev. B* 68 (2003) p.205201  
33  
34 [5] M. Ishimaru, I. T. Bae, A. Hirata, Y. Hirotsu, J. A. Valdez and K. E. Sickafus, *Nucl. Instrum.*  
35 *Meth. Phys. Res. B* 242 (2006) p.473-475  
36  
37 [6] M. Ishimaru, I. T. Bae, Y. Hirotsu, S. Matsumura and K. E. Sickafus, *Phys. Rev. Lett.* 89  
38 (2002) p.055502  
39  
40 [7] R. Devanathan, F. Gao and W. J. Weber, *Appl. Phys. Lett.* 84 (2004) p.3909-3911  
41  
42 [8] A. Mattausch, M. Bockstedte and O. Pankratov, *Phys. Rev. B* 69 (2004) p.235202  
43  
44 [9] A. Mattausch, M. Bockstedte and O. Pankratov, *Mater. Sci. Forum* 457-460 (2004) p.449  
45  
46 [10] J. M. Lento, L. Torpo, T. E. M. Staab and R. M. Nieminen, *J. Phys.: Condens. Matter* 16  
47 (2004) p.1053-1060  
48  
49  
50  
51  
52  
53  
54  
55  
56  
57  
58  
59  
60

- 1  
2  
3  
4  
5  
6  
7  
8  
9  
10  
11  
12  
13  
14  
15  
16  
17  
18  
19  
20  
21  
22  
23  
24  
25  
26  
27  
28  
29  
30  
31  
32  
33  
34  
35  
36  
37  
38  
39  
40  
41  
42  
43  
44  
45  
46  
47  
48  
49  
50  
51  
52  
53  
54  
55  
56  
57  
58  
59  
60
- [11] E. J. Bylaska, K. Tsemekhman and F. Gao, Phys. Scr. T124 (2006) p.86-90
- [12] M. Salvador, J. M. Perlado, A. Mattoni, F. Bernardini and L. Colombo, J. Nucl. Mater. 329-333 (2004) p.1219-1222
- [13] T. T. Petrenko, T. L. Petrenko and V. Y. Bratus, J. Phys.: Condens. Matter 14 (2002) p.12433-12440
- [14] A. Janotti and C. G. Van de Walle, Appl. Phys. Lett. 87 (2005) p.122102
- [15] J. Lægsgaard and K. Stokbro, Phys. Rev. Lett. 86 (2001) p.2834-2837
- [16] S. B. Zhang and J. E. Northrup, Phys. Rev. Lett. 67 (1991) p.2339-2342
- [17] S. B. Zhang, S. H. Wei and A. Zunger, Phys. Rev. B 57 (1998) p.9642-9456
- [18] A. F. Kohan, G. Ceder, D. Morgan and C. G. Van de Walle, Phys. Rev. B 61 (2000) p.15019-15027
- [19] Giannozzi P *et al.* <http://www.quantum-espresso.org>
- [20] J. M. Soler *et al.*, J. Phys.: Condens. Matter 14 (2002) p.2745-2779
- [21] N. Troullier N and J. L. Martins, Phys. Rev. B 43 (1991) p.1993-2006
- [22] J. Junquera, O. Paz, D. Sánchez-Portal and E. Artacho, Phys. Rev. B 64 (2001) p.235111
- [23] J. Shim, E. K. Lee, Y. J. Lee and R. M. Nieminen, Phys. Rev. B 71 (2005) p.245204
- [24] G. Makov, R. Shah and M. C. Payne, Phys. Rev. B 53 (1996) p.15513-15517
- [25] J. P. Crocombette, F. Jollet, L. Thien Nga and T. Petit, Phys. Rev. B 64 (2001) p.104107
- [26] G. Henkelman, B. P. Uberuaga, H. Jonsson, J. Chem. Phys. 113 (2000) 9901-9904
- [27] [N. Marzari \*et al.\*, Phys. Rev. Lett. 82 \(1999\) p.3296-3299](#)
- [28] A. Mattausch, Ph. D. Thesis, Friedrich-Alexander-Universität Erlangen-Nürnberg (2005)

Formatted: Font: Italic

Deleted: [27]

Deleted: ¶



**Table 1.** Comparison of results for bulk cubic SiC and for two interstitials configurations obtained with plane waves and with three different local orbital basis sets (see the text for details). The (Si-rich) formation energies were calculated with 65 atoms supercells and full atomic positions and cell volume relaxation.

Basis set	Energy	Mesh	A0	B0	$E_f(\text{ISi}_{\text{spc110}})$	$E_f(\text{ISi}_{\text{TC}})$
	shift	Cutoff	[Bohr]	[kbar]	[eV]	[eV]
<u>Localised</u> DZP	0.34 eV	80 Ry	8.23	2256	8.6	9.6
<u>Localised</u> TZ	0.10 eV	90 Ry	8.28	2226	10.7	13.4
<u>Localised</u> TZP	0.05 eV	90 Ry	8.16	2223	8.6	9.2
Plane Waves	-	-	8.21	2230	8.4	9.0

Formatted: Font: Italic

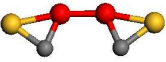
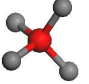
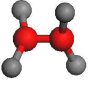
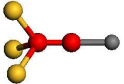
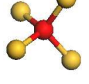
Formatted: Font: Italic

Deleted: ¶

Deleted: ¶

Formatted: Line spacing: Double

**Table 2.** Summary of silicon interstitials in order of decreasing relative stability for 3C-SiC, including the relaxed structure, the relevant bond lengths and the relative volume changes of the supercell ( $\Omega$ ), the crystallographic symmetry and their formation energies under C-rich and Si-rich conditions. <sup>a</sup>plane waves (PWSCF code) <sup>b</sup>(localised orbitals) SIESTA code <sup>c</sup>Lento *et al.* [7] <sup>d</sup>Bylaska *et al.* [8] <sup>e</sup>Bockstedte *et al.* [6] <sup>f</sup>Salvador *et al.* [9]

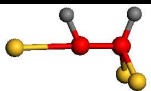
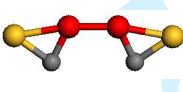
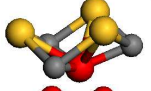
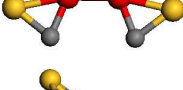
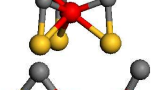
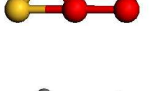
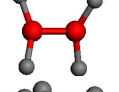
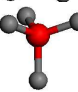
Defect	Structure	Distance (Å)	$E_f$ (C-rich) (eV)	$E_f$ (Si-rich) (eV)	$\Delta\Omega$ (%)	Symmetry
$I_{\text{Sisp}<110>}$		(Si-Si) <sub>sp</sub> :2.13; Si-Si:2.31 Si-C:1.77	8.86 <sup>a</sup> 9.12 <sup>b</sup>	8.40 <sup>a</sup> 8.59 <sup>b</sup> 7.4 <sup>c</sup> 8.5 <sup>e</sup>	1.85 <sup>a</sup> 2.29 <sup>b</sup>	$C_{2v}$
$I_{\text{TC}}$		Si-C:1.84	9.43 <sup>a</sup> 10.07 <sup>b</sup>	8.98 <sup>a</sup> 9.55 <sup>b</sup> 6.0 <sup>c</sup> 7.65 <sup>d</sup> 7.34 <sup>f</sup>	0.99 <sup>a</sup> 1.28 <sup>b</sup>	$T_d$
$I_{\text{Sisp}<100>}$		(Si-Si) <sub>sp</sub> :2.03; Si-C:1.79	10.23 <sup>a</sup> 10.42 <sup>b</sup>	9.78 <sup>a</sup> 9.90 <sup>b</sup> 9.83 <sup>d</sup>	2.43 <sup>a</sup> 2.84 <sup>b</sup>	$D_{2d}$
$I_{\text{Sisp}<111>}$		(Si-Si) <sub>sp</sub> :2.06; Si-Si:2.24 Si-C:1.71	11.04 <sup>a</sup> 11.41 <sup>b</sup>	10.58 <sup>a</sup> 10.88 <sup>b</sup>	1.62 <sup>a</sup> 2.05 <sup>b</sup>	$C_{3v}$
$I_{\text{TSi}}$		Si-Si:2.17	11.30 <sup>a</sup> 11.75 <sup>b</sup>	10.85 <sup>a</sup> 11.22 <sup>b</sup> 8.4 <sup>c</sup> 7.84 <sup>d</sup> 9.45 <sup>f</sup>	1.29 <sup>a</sup> 1.60 <sup>b</sup>	$T_d$

**Table 3.** Summary of silicon interstitials for 4H-SiC, from most to less stable, including the relaxed structure, the relevant bond lengths and the relative volume changes, the crystallographic symmetry and their formation energies under C-rich and Si-rich conditions.

<sup>a</sup> plane waves (PWSCF code) <sup>b</sup> localised orbitals (SIESTA code) <sup>c</sup> Mattausch [28]

Deleted: P

Deleted: [27]

Defect	Structure	Distance (Å)	$E_f$ (C-rich) (eV)	$E_f$ (Si-rich) (eV)	$\Delta\Omega$ (%)	Symmetry
$I_{sp<110>hex}$		(Si-Si) <sub>sp</sub> :2.15; Si-Si:2.34; Si-C:1.77	10.05 <sup>a</sup> 9.51 <sup>b</sup>	9.57 <sup>a</sup> 8.99 <sup>b</sup> 9.03 <sup>c</sup>	2.15 <sup>a</sup> 2.08 <sup>b</sup>	$C_s$
$I_{sp<10\bar{1}0>cub}$		(Si-Si) <sub>sp</sub> :2.10; Si-Si:2.27; Si-C:1.77	10.60 <sup>a</sup> 10.08 <sup>b</sup>	10.12 <sup>a</sup> 9.56 <sup>b</sup>	2.22 <sup>a</sup> 2.20 <sup>b</sup>	$C_s$
$I_{Hex(CSi)}$		Si-C:1.87; Si-Si:2.30	10.61 <sup>a</sup> 10.19 <sup>b</sup>	10.13 <sup>a</sup> 9.67 <sup>b</sup>	1.82 <sup>a</sup> 1.81 <sup>b</sup>	$C_{3v}$
$I_{sp<10\bar{1}0>hex}$		(Si-Si) <sub>sp</sub> :2.12; Si-Si:2.25; Si-C:1.79	10.67 <sup>a</sup> 10.08 <sup>b</sup>	10.19 <sup>a</sup> 9.55 <sup>b</sup>	2.28 <sup>a</sup> 2.23 <sup>b</sup>	$C_s$
$I_{Hex}$		Si-C:1.86-1.87; Si-Si:2.32-2.34	10.77 <sup>a</sup> 10.39 <sup>b</sup>	10.30 <sup>a</sup> 9.86 <sup>b</sup>	1.82 <sup>a</sup> 1.81 <sup>b</sup>	$C_{3v}$
$I_{sp<110>cub}$		(Si-Si) <sub>sp</sub> :2.01; Si-Si:2.28; Si-C:1.74-1.78	10.92 <sup>a</sup> 10.39 <sup>b</sup>	10.44 <sup>a</sup> 9.87 <sup>b</sup> 9.37 <sup>c</sup>	2.46 <sup>a</sup> 2.37 <sup>b</sup>	$C_s$
$I_{sp<100>cub}$		(Si-Si) <sub>sp</sub> :2.02; Si-C:1.76-1.83	11.19 <sup>a</sup> 10.66 <sup>b</sup>	10.71 <sup>a</sup> 10.14 <sup>b</sup>	2.67 <sup>a</sup> 2.61 <sup>b</sup>	$C_s$
$I_{TCcub}$		Si-C:1.83-1.86	12.12 <sup>a</sup> 11.98 <sup>b</sup>	11.64 <sup>a</sup> 11.46 <sup>b</sup>	1.52 <sup>a</sup> 1.53 <sup>b</sup>	$C_{3v}$

Deleted: ¶

**Figure 1** (Colour online) The investigated initial configurations of silicon interstitials in 3C-SiC (The split interstitials on carbon site are not displayed for brevity). The  $\langle 111 \rangle$  direction is normal to the page.

From left to right:  $I_{TSi}$   $I_{Cent}$   $I_{TC}$   $I_{Sisp\langle 100 \rangle}$   $I_{Sisp\langle 110 \rangle}$   $I_{Sisp\langle 111 \rangle}$   $I_{Hex(side+front)}$

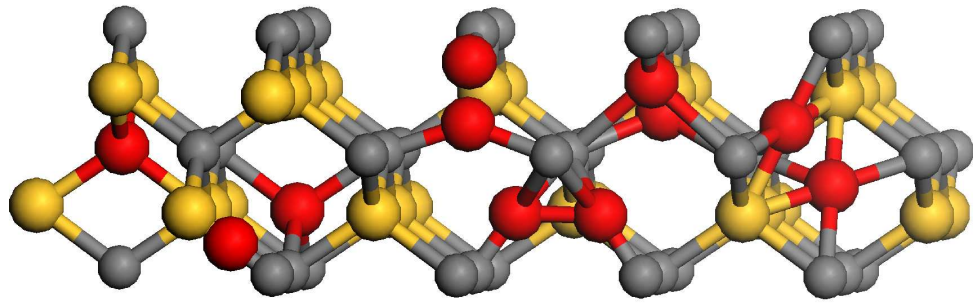
**Figure 2** (Colour online) Convergence of the formation energy of two types of silicon interstitials,  $I_{TC}$  and  $I_{Sisp\langle 110 \rangle}$ , in 3C-SiC with respect to different k-point samplings (a) ( $n+1/2$  x values corresponds to shifted k-point meshes), for the 65- and 129-atom supercells; convergence with respect to the increasing cell sizes (b), for  $\Gamma$  and converged k-points mesh, respectively.

**Figure 3** Energy path for the migration from  $I_{Sisp\langle 110 \rangle}$  to  $I_{TC}$  (from left to right) in 3C-SiC. Empty symbols represent points calculated with smearing of the Fermi surface, filled symbols were calculated with filled occupations. Lines are a guide to the eye.

**Figure 4** (Colour online) The investigated initial configurations of silicon interstitials in 4H-SiC. Configurations labels from left to right follow.  $\langle 1\bar{2}10 \rangle$  direction is normal to the page.

Cubic (upper) layer:  $I_{TSicub}$   $I_{TCcub}$   $I_{Sisp\langle 100 \rangle}$   $I_{Sisp\langle 110 \rangle}$   $I_{Sisp\langle 10\bar{1}0 \rangle}$   $I_{Sisp\langle 1\bar{2}10 \rangle}$   
 Hexagonal (lower) layer:  $I_{TCSi}$   $I_{Hex}$   $I_{Hex(CSi)}$   $I_{Sisp\langle 100 \rangle}$   $I_{Sisp\langle 110 \rangle}$   $I_{Sisp\langle 10\bar{1}0 \rangle}$   $I_{Sisp\langle 1\bar{2}10 \rangle}$

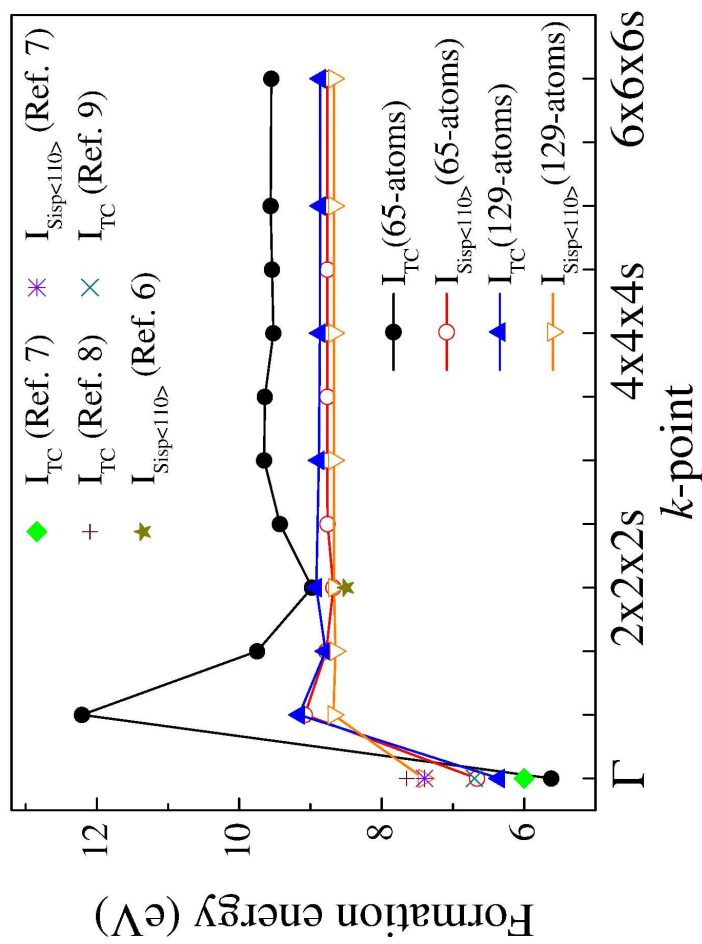
1  
2  
3  
4  
5  
6  
7  
8  
9  
10  
11  
12  
13  
14  
15  
16  
17  
18  
19  
20  
21  
22  
23  
24  
25  
26  
27  
28  
29  
30  
31  
32  
33  
34  
35  
36  
37  
38  
39  
40  
41  
42  
43  
44  
45  
46  
47  
48  
49  
50  
51  
52  
53  
54  
55  
56  
57  
58  
59  
60



128x52mm (352 x 352 DPI)

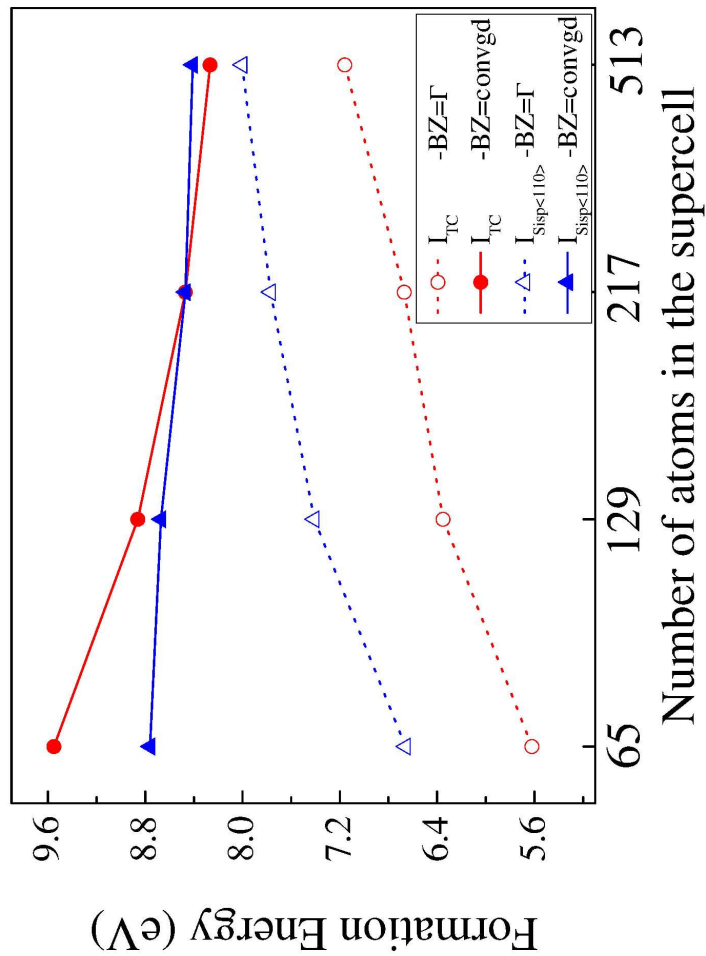
Peer Review Only

1  
2  
3  
4  
5  
6  
7  
8  
9  
10  
11  
12  
13  
14  
15  
16  
17  
18  
19  
20  
21  
22  
23  
24  
25  
26  
27  
28  
29  
30  
31  
32  
33  
34  
35  
36  
37  
38  
39  
40  
41  
42  
43  
44  
45  
46  
47  
48  
49  
50  
51  
52  
53  
54  
55  
56  
57  
58  
59  
60

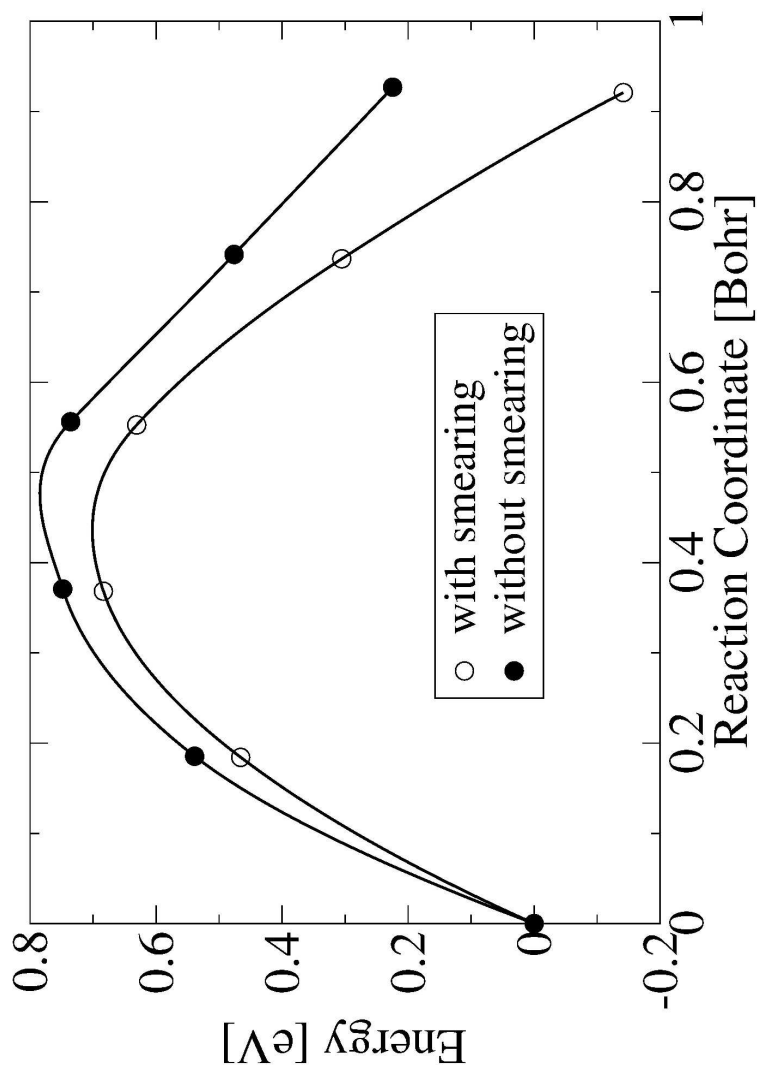


209x297mm (600 x 600 DPI)

1  
2  
3  
4  
5  
6  
7  
8  
9  
10  
11  
12  
13  
14  
15  
16  
17  
18  
19  
20  
21  
22  
23  
24  
25  
26  
27  
28  
29  
30  
31  
32  
33  
34  
35  
36  
37  
38  
39  
40  
41  
42  
43  
44  
45  
46  
47  
48  
49  
50  
51  
52  
53  
54  
55  
56  
57  
58  
59  
60



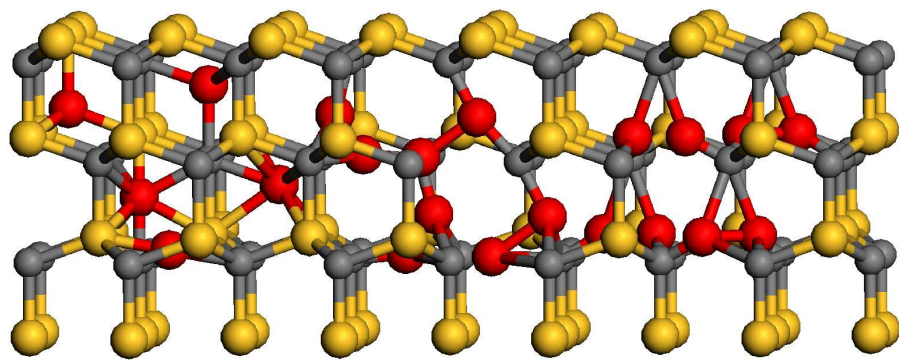
209x297mm (600 x 600 DPI)



215x279mm (600 x 600 DPI)



1  
2  
3  
4  
5  
6  
7  
8  
9  
10  
11  
12  
13  
14  
15  
16  
17  
18  
19  
20  
21  
22  
23  
24  
25  
26  
27  
28  
29  
30  
31  
32  
33  
34  
35  
36  
37  
38  
39  
40  
41  
42  
43  
44  
45  
46  
47  
48  
49  
50  
51  
52  
53  
54  
55  
56  
57  
58  
59  
60



135x58mm (322 x 322 DPI)

Pre-Review Only